MATERIALS CHEMISTRY FRONTIERS

REVIEW

View Article Online
View Journal | View Issue

Cite this: *Mater. Chem. Front.*, 2024, **8**, 1792

Tandem solar cells based on quantum dots

Juncheng Zhu,[ab] Kunyuan Lu,[a] Jing Li,[ac] Zeke Liu *[ab] and Wanli Ma [ab]

Establishing tandem photovoltaic device structures to achieve full-spectrum utilization of solar energy is a vital pathway to maximizing the power conversion efficiency (PCE). The dominant photovoltaic materials currently available (including silicon, perovskite, and organic semiconductors) are restricted by their bandgaps. They are only capable of utilizing the photon energy in the solar spectrum that is less than ~1100 nm. This limits the potential for further enhancements in device efficiency. Meanwhile, at present, the production process for infrared photovoltaic materials, represented primarily by III–V group semiconductors, is complex and costly, constraining their application in the field of civilian photovoltaic cells. Lead chalcogenide (PbX, X = S, Se) quantum dots (QDs) exhibit strong quantum confinement effects, and their bandgap can cover the entire infrared spectrum of solar light by adjusting their size. They can also be prepared through a solution process, denoting them as highly promising low-cost infrared photovoltaic materials. These are anticipated to serve as bottom cell materials in the construction of efficient, low-cost, tandem solar cells. In this paper, we provide a comprehensive summation of the latest research progress and challenges concerning various tandem solar cells based on QD materials (including QD/QD, organic/QD, and perovskite/QD). We aspire to highlight the immense potential of low-bandgap QD photovoltaic materials in the development of high-efficiency, stable, and cost-effective solar cells.

Received 7th October 2023,
Accepted 6th February 2024

DOI: 10.1039/d3qm01087b

rsc.li/frontiers-materials

1. Introduction

With the continuous growth of global energy demand, solar cells have emerged as a vital choice for modern societal development, as a clean, sustainable and versatile green energy technology. However, single-junction solar cells suffer from photon absorption losses as they can only absorb a portion of the solar spectrum's energy, limiting their PCE.[5,6] To address

[a] *Institute of Functional Nano & Soft Materials (FUNSOM), Joint International Research Laboratory of Carbon-Based Functional Materials and Devices, Soochow University, Suzhou, 215123, Jiangsu, P. R. China. E-mail: zkliu@suda.edu.cn*
[b] *Jiangsu Key Laboratory of Advanced Negative Carbon Technologies, Soochow University, Suzhou, 215123, Jiangsu, P. R. China*
[c] *Shandong Provincial Liaocheng Eco-environment Monitoring Centre, Liaocheng, 252000, Shandong, P. R. China*

Juncheng Zhu

Juncheng Zhu is currently a Master's student under the supervision of Associate Professor Zeke Liu at Soochow University. He obtained his BS degree from Soochow University. His current research interest focuses on the device physics of quantum dot optoelectronics.

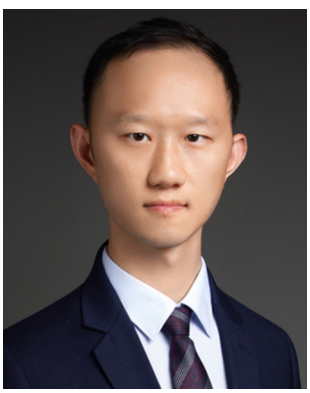

Wanli Ma

Zeke Liu is an associate professor at Soochow University. He obtained his PhD degree from Soochow University, and worked as a joint PhD student at the University of California, Berkeley and Lawrence Berkeley National Laboratory. Before he joined Soochow University in 2019, he worked as a joint postdoctoral scholar at Indiana University, Bloomington and Soochow University. His current research interest focuses on the design and synthesis of semiconductor quantum dots/nanocrystals, and their application in optoelectronic devices.

this issue, the tandem solar cell structure has been extensively studied. This structure consists of multiple subcells stacked with different bandgaps, allowing for the maximal utilization of photons from various wavelength ranges, thereby reducing thermalization and transmittance losses and enhancing the PCE beyond the Shockley–Queisser limit. The theoretical efficiency of two-junction solar cells can reach 45.8%, significantly surpassing the theoretical efficiency of single-junction cells at 31–33%.[8,9] For instance, perovskite materials can compensate for the light absorption losses in the high-energy region of silicon. Consequently, the fabrication of perovskite/silicon tandem devices has become a current research hotspot, with the highest PCE of monolithic devices reaching 33.7%.[12] Combined with the low-cost advantage inherent in perovskite's solution-based processing, perovskite/silicon tandem devices have embarked upon the journey of industrialization.[13,14] Meanwhile, perovskite/perovskite and perovskite/organic tandem solar cells prepared based on the solution method have also become a cutting-edge research direction in the field.[1,15–23] The energy range covered by the solar spectrum is approximately 0.5–4.4 eV (corresponding to wavelengths of 280–2500 nm), whereas silicon can only absorb photons with energies higher than 1.1 eV (corresponding to wavelengths below ~1100 nm), and narrow-bandgap perovskite can only absorb photons with energies greater than ~1.2 eV (corresponding to wavelengths below ~1000 nm).[29] Even with the construction of perovskite/silicon tandem devices, approximately 20% of the solar spectrum's energy remains unutilized.[32] To further enhance the PCE, it is crucial to fully capture the infrared energy in the solar spectrum. This goal has been achieved in III–V tandem devices, reaching a remarkable PCE of 47.6% through the combination of concentrator technology. This is also the highest certified efficiency among all solar cells published by the National Renewable Energy Laboratory (NREL), demonstrating the significant implications of harnessing infrared energy.[12] However, due to the rigorous fabrication processes and high production costs associated with III–V materials, their high-efficiency solar cells are primarily utilized in high-end specialized fields such as aerospace and military applications. Therefore, the development of low-cost narrow-bandgap infrared photovoltaic materials holds an immense application value.

Lead chalcogenide (PbS, X = S, Se) QDs represent a new generation of solution-processable photovoltaic materials, possessing the following characteristics: (1) they can be synthesized in large quantities through solution methods, enabling the preparation of conductive inks suitable for printing techniques such as blade coating and spray coating, thereby facilitating the fabrication of large-area thin films.[34–37] (2) Compared to other photovoltaic materials, PbX QDs, due to their strong quantum confinement effect, allow the tuning of their bandgap through size manipulation, enabling absorption across almost the entire solar spectrum (300–2500 nm).[32,38–42] Among the emerging low-cost solution-processable photovoltaic materials, PbX QDs are currently the only semiconductor materials capable of fully covering the infrared region of the solar spectrum. (3) By chemically modifying the QD surface, it is possible to adjust the doping type and carrier concentration of the QD films,[43–47] thereby precisely controlling their optoelectronic properties for improved application in photovoltaic devices. (4) PbS QD solar cells exhibit remarkable air stability, as unencapsulated devices can retain their efficiency almost unchanged after 7 years of storage in ambient air.[48,49] The recent development of direct synthesis methods for QD semiconductor inks has significantly reduced their production costs, making them highly suitable for industrial-scale applications.[37,50–55] Consequently, PbX QDs emerge as ideal low-cost narrow-bandgap photovoltaic material, holding promise as bottom cell materials for the fabrication of low-cost, high-efficiency, and highly stable tandem solar cells.

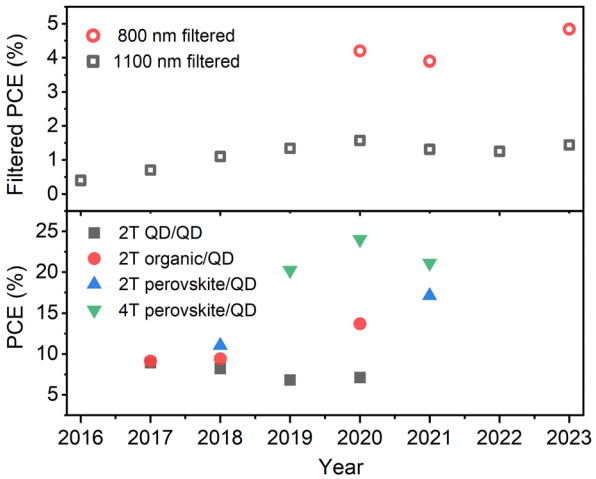

Fig. 1 Evolution of the maximum PCE per year for QD-based tandem solar cells and the maximum filtered PCE per year for infrared QD cells reported in the literature. The 800 nm filtered and 1100 nm filtered devices donate simulated 4T perovskite/QD and 4T silicon/QD tandem solar cells, respectively.

In this review, we endeavor to provide a comprehensive exploration of the recent research progress and challenges surrounding tandem solar cells based on QDs. We will commence by introducing the fundamental architecture and operational principles of tandem solar cells. Subsequently, we will delve into a detailed discussion of the research progress pertaining to three distinct types of tandem solar cells: QD/QD, organic/QD, and perovskite/QD (Fig. 1). Lastly, in the concluding and prospective section, we will offer insights into the future development of tandem solar cells based on QDs, along with an exploration of potential challenges and corresponding solutions. Through this review, we aspire to provide readers with a comprehensive and profound understanding of tandem solar cells based on PbS QDs, while providing reference and inspiration for researchers dedicated to developing low-cost, stable and efficient solar cells.

2. Tandem architectures and working principles

This section will expound upon the fundamental architecture and operational principles of tandem solar cells. Tandem solar

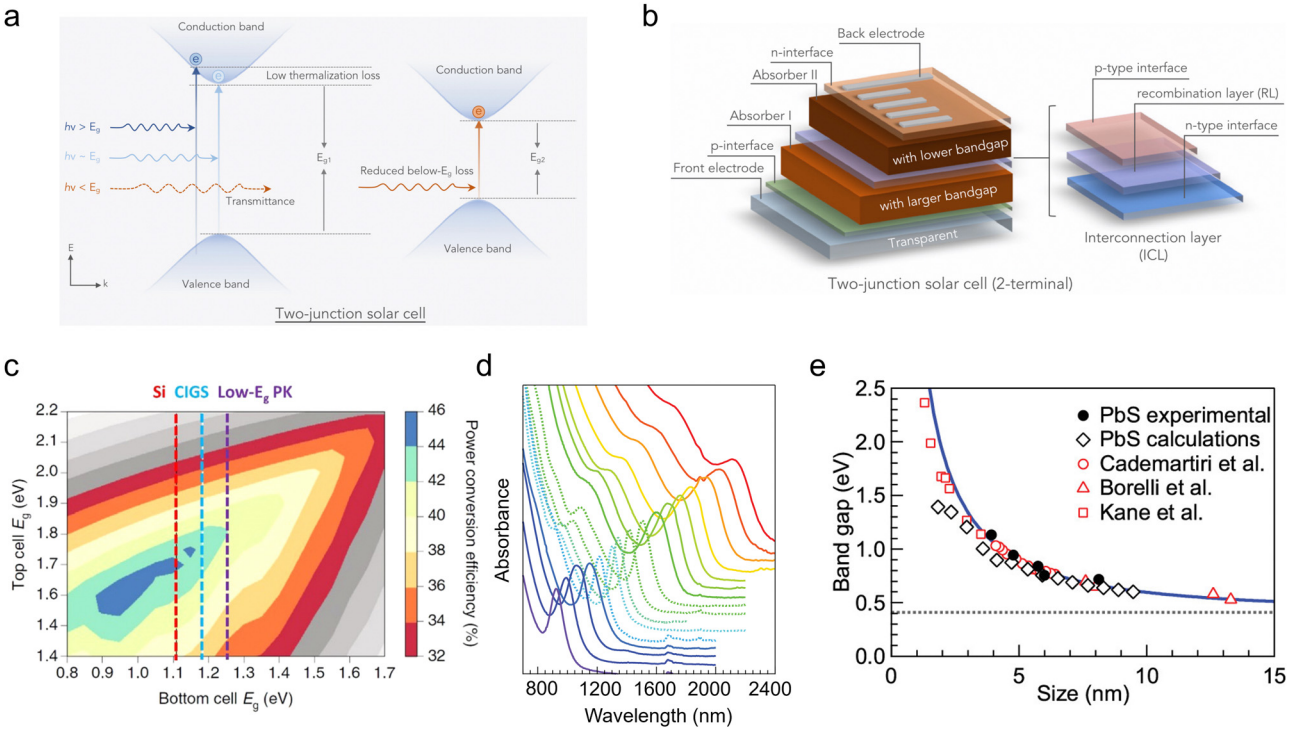

Fig. 2 (a) Band diagram of the thermalization loss and below-band-gap loss. (b) Typical device structure for two-junction solar cells.[1] Reprinted with permission. Copyright 2023 Cell Press. (c) Schematic diagram illustrating the relationship between the theoretical PCE limit and the bandgap of sub-cells in 2T tandem solar cells.[7] Reprinted with permission. Copyright 2019 IOP Publishing Ltd. (d) Typical absorbance spectra of PbS QD suspensions.[24] Reprinted with permission. Copyright 2011 American Chemical Society. (e) Relation between the PbS QD band gap and the particle size.[28] Reprinted with permission. Copyright 2009 American Chemical Society.

cells primarily consist of two or more independent subcells, which segmentally absorb sunlight through multiple semiconductor layers with varying bandgaps. This design aims to mitigate carrier thermal relaxation losses in low-bandgap cells when absorbing high-energy photons, maximizing the utilization of the solar spectrum and thereby enhancing the device's open-circuit voltage (V_{OC}) and PCE (Fig. 2(a)).[7]

The two-junction tandem structure represents the most emblematic and pragmatic tandem photovoltaic technology. Thus, in this review, our emphasis will be placed on two-junction tandem cells. This configuration comprises a top cell with a wide bandgap and a bottom cell with a narrow bandgap. The top cell absorbs high-energy photons, while the bottom cell absorbs low-energy photons.[7] Two-junction tandem cells are primarily implemented in two configurations: two-terminal (2T) and four-terminal (4T) tandem architectures.

A 2T tandem solar cell is formed by connecting two subcells in series on the same substrate (Fig. 2(b)). These subcells can adopt either a conventional or an inverted structure. They share a common transparent front electrode and an opaque back electrode, connected optically and electrically by an interlayer.[7] This interlayer may consist of a tunnel junction made from the hole transport and electron transport layers of the two subcells or a recombination layer that includes transparent conductive oxides (TCOs) or ultra-thin metals paired with carrier transport layers. The latter is more commonly used in QD 2T tandem solar cells. Within the recombination layer, electrons and holes extracted from the top and bottom cells recombine, while the respective electrodes collect the remaining charges to generate a photocurrent.[56]

The design of the recombination layer must adhere to three main principles: (1) selecting materials with suitable work functions to form ohmic contacts with the carrier transport layers of each subcell; (2) with high carrier mobility to facilitate charge recombination within the recombination layer; and (3) managing the thickness and lateral conductivity of the recombination layer to prevent short-circuiting caused by extensive plane conduction from the top subcell to the bottom one. Notably, after surface ligand treatment, QDs not only act as carrier transport layers but also allow for the tuning of work functions, greatly simplifying the recombination layer's design.[57]

During the fabrication process, it is crucial to carefully manage the conditions for processing the recombination layer in order to prevent any damage to the active layer of the bottom subcell due to high energy or temperature. Additionally, the recombination layer must remain stable during the top subcell's fabrication, unaffected by subsequent processes. Finally, in solution-processed tandem solar cells, particularly during the fabrication of the PbS QD top subcell, the small molecule ligand exchange step can potentially damage underlying layers. Therefore, the recombination layer should also serve as an

Table 1 Advantages and disadvantages of 2T and 4T tandem devices

	2T	4T
Advantages	• Simple structural design • Low parasitic resistance and minimal optical loss • Reduced manufacturing costs due to fewer electrodes and deposition steps	• Simple fabrication process • No current matching constraints for sub-cells • Independent operation and optimization of sub-cells
Disadvantages	• Require current matching between sub-cells • High material selection standards for the active layers and interconnecting layers	• Optical losses due to parasitic absorption • Additional costs for extra transparent electrodes, inverters and cables

effective barrier to material interdiffusion, preventing solvent penetration and protecting the bottom subcell.[57]

The advantages of the 2T tandem solar cell lie in its simple structure, resulting in lower parasitic resistance and minimal optical losses, thereby exhibiting greater potential for practical efficiency (Table 1). Moreover, it requires less material usage and deposition steps, leading to reduced manufacturing costs.[58] However, the tandem structure necessitates equal currents from each subcell. Otherwise, the efficiency of the 2T tandem solar cell will be compromised by the subcell with a lower photocurrent. This requirement raises the standards for designing active layer materials. It is critical to ensure that the bandgaps of the materials in both subcells match well. Additionally, other crucial factors like optical absorption coefficients, carrier lifetimes, and diffusion lengths must be taken into account to ascertain the ideal layer thickness for achieving current matching. Additionally, the processing of the recombination layer and the second cell is constrained by factors such as cell polarity, substrate roughness, deposition temperature, solvent compatibility, and other considerations, making the fabrication process more challenging.[58]

The 4T tandem solar cell can be formed by mechanically stacking two independent subcells or assembling them with an optical splitting system.[7] Each subcell possesses positive and negative electrodes, electrically isolated from each other, enabling independent operation and optimization. In comparison to 2T cells, 4T cells feature four electrodes, with at least three of them requiring both transparency with a wide bandgap and high conductivity.[59] This tandem cell offers simplicity in fabrication and eliminates the constraints of current matching. During operation, the two subcells can be individually maintained at their maximum power points, benefiting from separate tracking systems. This reduces restrictions on top cell bandgap selection and enhances the system's insensitivity to spectral variations.[58] However, this also implies the necessity of bearing additional costs for inverters, wiring, and other related equipment.[7] Moreover, the inclusion of two intermediate electrodes and insulating separation layers has augmented its manufacturing expenses and introduced significant optical losses due to additional absorption or reflection.[59]

In 2T tandem solar cells, the short-circuit current density (J_{SC}) is determined by the minimum current generated in the two sub-cells, while the V_{OC} of a well-functioning device is the sum of the V_{OC} of both sub-cells. There is no direct correlation between the fill factor (FF) of tandem cells and that of single-junction devices. Nonetheless, defects and shunt resistance in the sub-cell with a lower current can affect the FF of the tandem device to a large extent.[60] To realize efficient 2T tandem devices, various factors such as optical and electrical matching between sub-cells, interlayer reflection, and absorption losses require comprehensive consideration. Ideally, if each sub-cell achieves bandgap matching and extends the range of solar spectrum utilization, the efficiency of the 2T tandem cells should surpass that of single junction sub-cells.

For 4T tandem solar cells, the two sub-cells can be optimized and function independently, without the constraint of current matching, thus their PCE is typically the sum of the efficiencies of the two filtered sub-cells. This offers greater flexibility in the design and optimization of 4T solar cells.

Fig. 2(c) illustrates the dependence of the theoretical PCE of two-junction solar cells in the monolithic 2T configurations as a function of the bottom and top cell bandgap. The primary challenge in achieving highly efficient tandem solar cells lies in identifying semiconductor materials with appropriate bandgaps.

The theoretical calculation indicates the maximum PCE of two-junction tandem solar cells can reach 45.8% by integrating two subcells with bandgaps of 1.6 eV and 0.95 eV, respectively.[24,28,38,61–63] Colloidal PbX QDs can accomplish bandgap tuning from 0.6 to 2.4 eV by changing their size, fully covering the requirement for tandem solar cells (Fig. 2(d) and (e)). Therefore, QD has always been considered one of the ideal photovoltaic materials for constructing tandem solar cells.

3. QD/QD tandem solar cells

As demonstrated above, PbX QDs with different bandgaps can be obtained by size control, which can easily meet the bandgap requirements of tandem solar cells. Therefore, the research on QD/QD tandem solar cells has attracted attention at an early stage.

In 2011, Choi *et al.* reported the first solution-processed QD/QD tandem solar cell (Fig. 3(a)).[3] Leveraging the quantum confinement effect, they achieved the desired energy bandgap by precisely controlling the size of PbS QDs. The recombination layer ZnO/Au/poly(3,4-ethylenedioxythiophene):poly(styrenesulfonate) (PEDOT:PSS) was employed, successfully improving the V_{OC} compared to the subcells, despite the limited PCE of only 1.27%. In the same year, Wang *et al.* devised a gradient recombination layer comprising four oxide materials: MoO_3/ITO/aluminum-doped ZnO (AZO)/TiO_2 (Fig. 3(b)). This design allows matched electron and hole currents to meet and

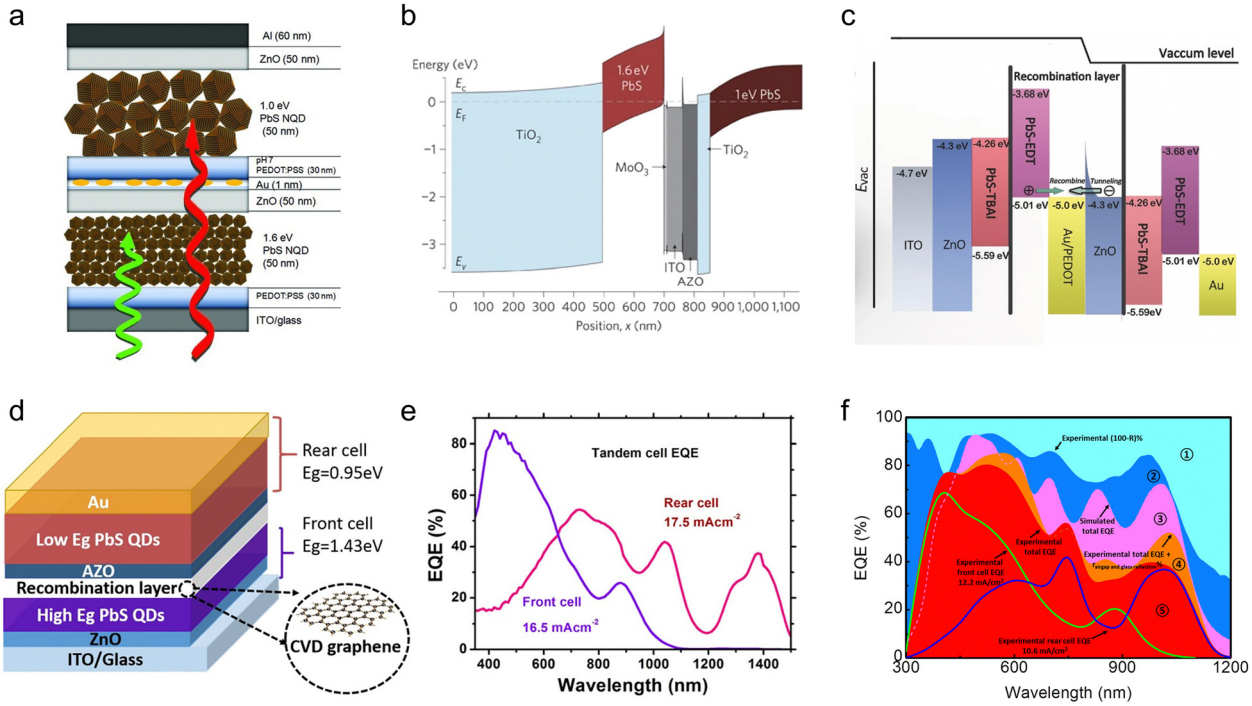

Fig. 3 (a) Device structure of the first solution-processed 2T all-quantum-dot tandem solar cell.[3] Reprinted with permission. Copyright 2011 Wiley-VCH Verlag GmbH & Co. KGaA, Weinheim. (b) Energy level alignment of the 2T all-quantum-dot tandem solar cell with a gradient recombination layer composed of four oxide layers.[11] Reprinted with permission. Copyright 2011, Springer Nature Limited. (c) Energy level alignment of the 2T all-quantum-dot tandem solar cell based on solution-processed recombination layers and highly efficient all-inorganic recombination layers.[26] Reprinted with permission. Copyright 2017 Wiley-VCH Verlag GmbH & Co. KGaA, Weinheim. (d) Device structure and (e) EQE curves of the 2T all-quantum-dot tandem solar cell with graphene as the recombination layer.[31] Reprinted with permission. Copyright 2018 American Chemical Society. (f) EQE curves of the 2T all-quantum-dot tandem solar cell with optimized quantum dot size and active layer thickness based on optical simulations.[33] Reprinted with permission. Copyright 2019 American Chemical Society.

recombine. As a result, the tandem device exhibited a V_{OC} of 1.06 V, equal to the sum of subcells' voltage, and realized a PCE exceeding 4%.[11] However, the process of depositing the four functional layers through sputtering technology added complexity to the fabrication process. In 2017, Crisp *et al.* employed CdTe nanocrystals as the front cell and lead sulfide QDs as the back cell for tandem solar cells.[8] By utilizing the ZnTe–ZnO recombination layer, they achieved a V_{OC} of 1.1 V and a PCE of 5% in their optimized prototype device. In the same year, Shi *et al.* introduced a solution-processed recombination layer composed of PbS-EDT/PEDOT/ZnO (Fig. 3(c)), enabling the fabrication of tandem devices under ambient conditions. The corresponding device achieved an efficiency of 7.7%. They also devised an all-inorganic recombination layer consisting of PbS-EDT/Au/ZnO (Fig. 3(c)), significantly enhancing the efficiency of PbS QD tandem cells to 9%, with a V_{OC} of 1.13 V. More importantly, the tandem device shows excellent air stability.[26] The work employed PbS QDs with the same bandgap for the subcells, which limits the device performance. In 2018, Bi *et al.* made an unprecedented stride by introducing graphene as the recombination layer for QD/QD tandem solar cells (Fig. 3(d) and (e)). This innovative approach relies on chemical vapor deposition rather than vacuum-deposition based IML in previous works. This approach can simplify the fabrication process and reduce costs, while achieving an impressive PCE of up to 8.2%.[31]

So far, the development of QD/QD tandem solar cells has significantly lagged behind that of their single-junction counterparts. The device parameters of reported QD/QD tandem solar cells are presented in Table 2. PbX QDs exhibit a higher absorption coefficient across the visible spectrum compared to the near-infrared range. They also suffer from an absorption valley before the first exciton absorption peak. These features make it difficult to achieve ideal absorption complementarity in QD/QD tandem solar cells. This limitation, coupled with the inherent drawback of high surface trap density in QDs, poses a significant challenge to the overall device performance. Future research efforts can focus on enhancing current matching by carefully optimizing the QD bandgap and thickness (Fig. 3(f)),[33] or by integrating QDs with other types of photovoltaic materials. Furthermore, the lower absorption coefficients of QD materials in the infrared spectrum, particularly at the valley before the first exciton absorption peak, contribute to reduced current values in the infrared range. This poses an additional challenge in achieving current matching with the top subcells. Enhancing the absorption capacity of QDs in the infrared region through the optical design of the device may be one way to overcome this challenge. For instance, Baek *et al.* achieved structured back electrodes by embossing the polymer hole transport layer, which effectively improved the external quantum efficiency (EQE) of PbS QDs at around a wavelength of 1200 nm.[64]

Table 2 Summary of 2T QD/QD tandem solar cells

Sub-cells	E_g [eV]	Absorbers	CRL	V_{OC} [V]	J_{SC} [mA cm^{-2}]	FF [%]	PCE [%]	Ref.
Front cell	1.6	PbS	ZnO/Au/PEDOT:PSS	0.91	3.7	37	1.27	3
Back cell	1	PbS						
Front cell	1.6	PbS	MoO_3/ITO/AZO/TiO_2	1.06	8.3	48	4.21	11
Back cell	1	PbS						
Front cell	1.5	CdTe	ZnTe/ZnO	1.06	9.9	45	4.7	8
Back cell	1	PbS						
Front cell	1.33	PbS	PbS-EDT/PEDOT/ZnO	1.02	12.92	58.5	7.7	26
Back cell	1.33	PbS						
Front cell	1.33	PbS	PbS-EDT/Au/ZnO	1.13	12.26	64.1	8.9	26
Back cell	1.33	PbS						
Front cell	1.4	PbS	Gr/AZO	1.12	12.38	59	8.2	31
Back cell	1.3	PbS						
Front cell	1.44	PbS	PbS-EDT/Au/ZnO	1.07	11.5	55	6.8	33
Back cell	1.22	PbS						
Front cell	1.45	PbS	PbS-EDT/NiO/Ag/ZnO	1.02	11.7	60	7.1	65
Back cell	1.22	PbS						
Front cell	1.45	PbS	PbS-EDT/NiO/Ag/ZnO	0.92	12.1	55	6.3	65
Back cell	0.97	PbS						

4. Organic/QD tandem solar cells

The tandem structure of organic/QD solar cells represents a novel photovoltaic device with immense potential, as it combines the unique advantages of organic semiconductors and QDs. QDs possess the tunable wide bandgap, enabling them to absorb a broad range of wavelengths from visible light to near-infrared. However, they suffer from low V_{OC} and relatively weak absorption before the first exciton absorption peak (~650–900 nm). On the other hand, organic solar cells exhibit narrow spectral absorption but a high V_{OC} value, and with appropriate material selection, they can also possess near-infrared absorption capabilities. Furthermore, both materials support solution-based processing. It is promising to fully exploit the solar spectrum and achieve high PCE through the adoption of an organic/QD tandem structure.

In 2014, Speirs *et al.* introduced the first solution-processed hybrid tandem solar cell with PbS QDs and P3HT:PCBM organic materials as the absorbing layer and Al/WO_3 as the recombination layer.[66] This device achieved an V_{OC} of 0.89 V, equivalent to 92% of the sum of the subcell voltages. However, due to the limited utilization of near-infrared light by the QD absorbing layer, its efficiency reached only 1.8%, even lower than the corresponding subcell. Then Kim *et al.* employed depletion of the heterojunction TiO_2/PbS QD and polymer bulk heterojunction PTB7:$PC_{71}BM$ as the absorbing layer, along with MoO_X/ZnO/poly[(9,9-bis(3′-(*N*,*N*-dimethylamino)propyl)-2,7-fluorene)-*alt*-2,7-(9,9-dioctylfluorene)] (PFN) as the recombination layer. They attained a high V_{OC} of 1.3 V and an impressive FF of approximately 70%, resulting in a PCE of 5.33% (Fig. 4(a)–(c)).[4] However, the lack of spectral complementarity between the two subcells led to a relatively low J_{SC} in the hybrid tandem device, and the overall PCE still remained below that of the individual subcells. Based on this work, Aqoma *et al.* precisely optimised the thickness ratio of two materials, achieving improved current density matching in subcells. Furthermore, they employed a recombination layer of MoO_X/Au/ZnO. As a result, a PCE of 8.27% in the hybrid tandem photovoltaic device was realized.[67] In the same year, Kim *et al.* utilized PDPP3T:$PC_{61}BM$ to replace the previous PTB7:$PC_{71}BM$, which effectively supplemented the insufficient absorption within the range of 650–900 nm in the PbS QD film. Combining it with a MoO_3/ultrathin Au/PFN recombination layer, they achieved a PCE of 7.9%.[68] Later, Li *et al.* proposed the utilization of aqueous vapor for the treatment of post-ligand exchange PbS QD layers, enabling the formation of interlayer oxides $PbSO_3$ and $PbSO_4$, thus preventing charge recombination between PbS QDs, consequently resulting in higher V_{OC} and FF.[68] Their hybrid tandem solar cell, with water vapor-treated PbS QD as the front cell and PTB7-Th:$PC_{71}BM$ as the back cell, achieved a PCE of 9.12%. In 2020, Aqoma *et al.* employed PTB7-Th:IEICO-4F organic back cells to enhance the absorption in the wavelength range of 350–1000 nm, further compensating for the insufficient absorption of PbS QDs in the valley region. Through the optimization of subcell J_{SC} balance and charge recombination, they achieved an impressive PCE of 12.82%.[69]

In the conventional design of hybrid tandem solar cells using QDs and organic materials, QDs are typically employed as the front cell, while organic materials serve as the back cell. This design inherently suffers from the drawback that incident light is primarily absorbed by the low-bandgap QD front cell, leaving only a small fraction of light energy absorbed by the organic back cell, leading to the photocurrent imbalance between the two subcells. However, altering this structure poses significant challenges since the fabrication of top QD subcells may damage the bottom organic subcell. To address this issue, Tong *et al.* reported a novel top-illuminated organic/QD hybrid tandem solar cell in 2017 (Fig. 4(d)–(f)).[10] They retained PbS QDs as the front cell and organic materials as the back cell. Particularly noteworthy is their utilization of the conductive polymer PEDOT:PSS as a transparent electrode at the top of the cell. This arrangement allows light to be illuminated through the transparent electrode, enabling the organic subcell to absorb light first and achieve a highly balanced

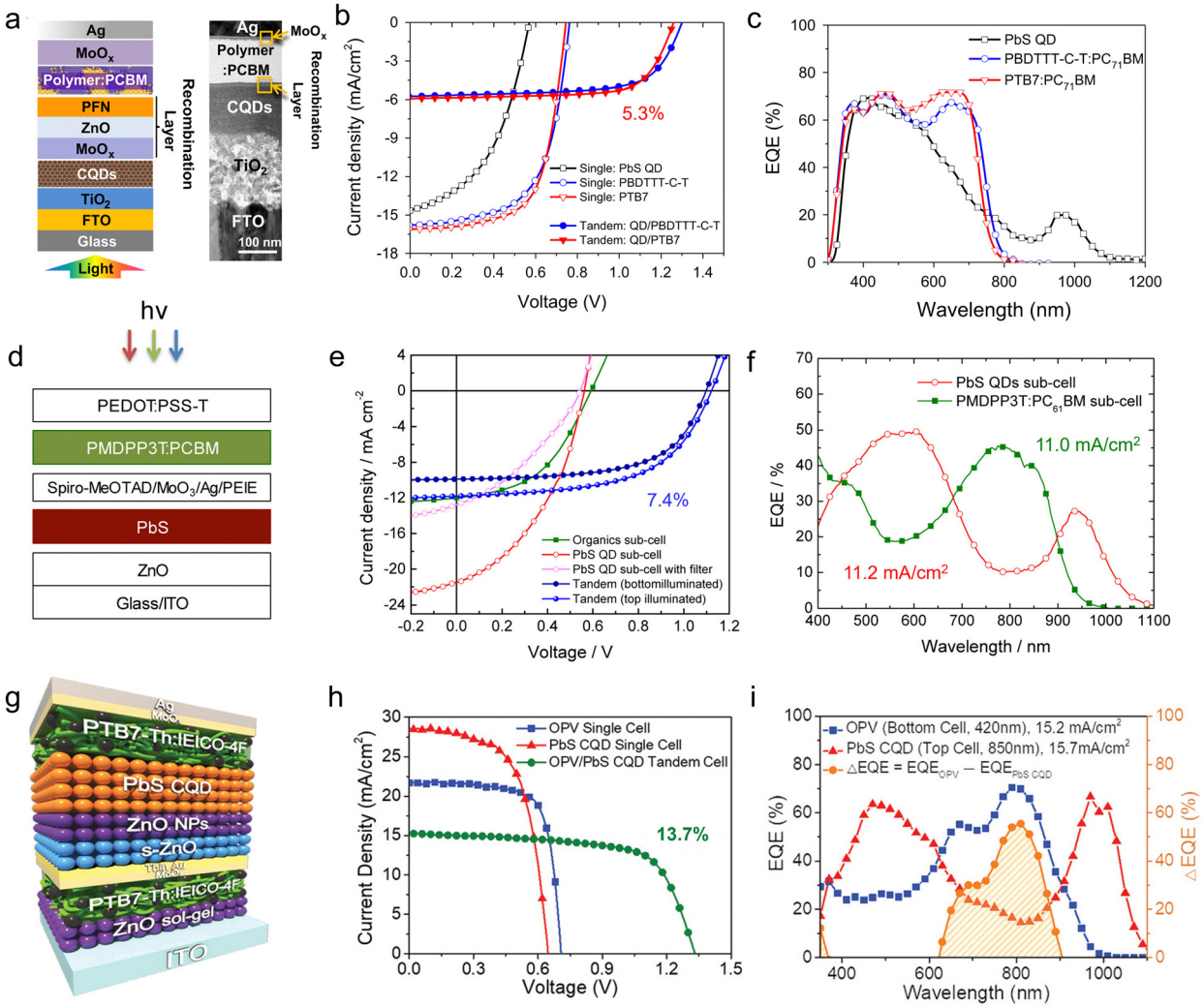

Fig. 4 (a) Device structure, (b) *J–V* and (c) EQE curves of early-stage 2T organic/QD tandem solar cells.[4] Reprinted with permission. Copyright 2015 Published by Elsevier Ltd. (d) Device structure, (e) *J–V*, and (f) EQE curves of novel top-illuminated 2T organic/QD tandem solar cells.[10] Reprinted with permission. Copyright 2017 American Chemical Society. (g) Device structure, (h) *J–V* and (i) EQE curves of the 2T organic/QD tandem solar cell using PTB7-Th:IEICO-4F organic sub-cells for further optimization of spectral absorption, based on organic materials as pre-cells and QDs as post-cells.[27] Reprinted with permission. Copyright 2020 Wiley-VCH GmbH.

Table 3 Summary of 2T organic/QD tandem solar cells

Sub-cells	E_g [eV]	Absorbers	CRL	V_{OC} [V]	J_{SC} [mA cm^{-2}]	FF [%]	PCE [%]	Ref.
Front cell	1.2	PbS	Al/WO_3	0.89	3.9	53	1.8	66
Back cell	1.6	P3HT:PCBM						
Front cell	1.28	PbS	MoO_X/ZnO/PFN	1.25	6.12	69.15	5.29	4
Back cell	1.84	PTB7:$PC_{71}BM$						
Front cell	1.3	PbS	MoO_X/Au/ZnO	1.27	10.36	63	8.27	67
Back cell	1.6	PTB7-Th:$PC_{71}BM$						
Front cell	1.38	PbS	Spiro-MeOTAD/MoO_3/Ag/PEIE	1.12	11.8	56	7.4	10
Back cell	1.3	PMDPP3T:$PC_{61}BM$						
Front cell	1.34	PbS	MoO_3/Au/PFN	1.25	9.3	67	7.9	68
Back cell	1.56	PDPP3T:$PC_{61}BM$						
Front cell	1.3	PbS	MoO_X/Au/ZnO	1.25	9.89	74.1	9.12	70
Back cell	1.6	PTB7-Th:$PC_{71}BM$						
Front cell	1.84	PTB7:$PC_{61}BM$	MoO_X/Au/AZO	1.31	12.5	56.7	9.4	71
Back cell	1.28	PbS						
Front cell	1.45	PbS	PbS-EDT/Au/ZnO	1.36	13.63	69	12.82	69
Back cell	1.6	PTB7-Th:IEICO-4F						
Front cell	1.6	PTB7-Th:IEICO-4F	MoO_X/Au/ZnO NPs/s-ZnO	1.34	15.2	67.4	13.7	27
Back cell	1.3	PbS						

photocurrent. The PCE of this hybrid device reached 7.4%, with a J_{SC} of 11.8 mA cm^{-2}. In 2018, Kim *et al.* improved the ink formulation of PbS QDs by replacing the commonly used solvents such as octane and butylamine with hexane.[71] This reduced the damage to the underlying structures. They also introduced a more robust MoO_X/Au/AZO recombination layer. With these modifications, they achieved a structure where organic materials served as the front cell and QDs as the back cell. The photocurrent of the device increased by approximately 20–25% compared to previously reported devices, resulting in a PCE of 9.4%. In 2020, Kim *et al.* further improved the reverse architecture consisting of the organic front cell and QD back cell.[27] They utilized PTB7-Th:IEICO-4F in combination with QDs, creating a dual near-infrared absorption system. They also introduced a sol–gel-ZnO/ZnO nanoparticle (NP) buffer layer to address the issue of QD solvent permeation into the underlying organic layer. The matched current of the hybrid tandem solar cell significantly increased to 15.2 mA cm^{-2}, resulting in a PCE of 13.7% (Fig. 4(g)–(i)), which is the highest reported PCE for organic/QD tandem solar cells (Table 3).

After nearly a decade of development, the efficiency of organic/QD tandem solar cells has increased from an initial range of 1–2% to over 13%. This progress can primarily be attributed to the complementary design of the two materials' absorption spectra, the balance of photocurrent, the engineering of intermediate recombination layers, and the innovative structural design. These crucial improvements have significantly enhanced the efficiency and performance of organic/QD tandem solar cells. Looking ahead, organic/QD tandem solar cells hold immense potential for further advancement. By continually optimizing the material system and interface engineering, it is believed that both the PCE and stability will experience substantial enhancements.

5. Perovskite/QD tandem solar cells

Metal halide perovskites have been considered as one of the ideal semiconductors for fabricating efficient and stable thin-film solar cells, due to their exceptional optoelectronic performance. In recent years, the certified efficiency of single-junction perovskite solar cells has reached 26.1%.[12] However, further enhancements in its efficiency present significant challenges. To overcome this limitation, researchers have begun exploring the tandem configuration of perovskite with other photovoltaic materials. Among these configurations, perovskite/silicon and perovskite/perovskite tandem devices have demonstrated impressive efficiency.[1,15–23] However, as mentioned earlier, such tandem cells are unable to harness low-energy photons (>1100 nm) from the solar spectrum. Furthermore, in order to achieve photocurrent matching, the use of mixed-composition perovskite materials is necessary, which results in decreased stability. On the other hand, constructing an infrared perovskite/QD tandem solar cell holds the potential for the following advantages:

(1) High theoretical efficiency: theoretical calculations indicate that the highest efficiency can be achieved for the two-junction tandem cell by serially connecting subcells with bandgaps of 1.6 eV and 0.95 eV. In contrast, the current research focuses on crystalline silicon with a bandgap of approximately 1.12 eV, and narrow-bandgap perovskites such as Pb/Sn mixtures with a bandgap of around 1.2 eV, both of which fail to attain the optimal bottom cell bandgap. The bandgap of PbS QDs can be tuned within the range of 0.6–2.4 eV by adjusting their size, thereby meeting the demands of ideal tandem solar cells for narrow-bandgap photovoltaic materials. The theoretical calculation indicates a PCE of up to 43% can be realized for perovskite/QD tandem solar cells under 1-sun illumination (Fig. 5(a) and (b)).[2]

(2) High stability: currently, the tandem devices based on perovskite require the utilization of mixed-composition perovskite materials. However, wide-bandgap perovskites prepared through halide mixing exhibit phase separation issues, especially under illumination, while narrow-bandgap perovskites fabricated *via* the Pb/Sn mixing strategy face challenges related to the easy oxidation of divalent tin ions. These factors significantly undermine the stability of tandem devices, posing immense challenges for practical applications. In contrast, it is possible to utilize single-component or near-single-component perovskite materials with superior stability in the perovskite/infrared QD tandem devices, due to the smaller bandgap of QDs. Moreover, the utilization of stable QDs as the top cell has the potential to provide protection for the underlying perovskite and to further enhance the stability of the entire tandem device.

(3) Low cost: both QD and perovskite materials can be scaled up through solution-processed methods, offering the potential for lower fabrication costs compared to perovskite/silicon tandem devices, while also being compatible with flexible substrates. Additionally, recent advancements in direct synthesis methods of PbX QD semiconductor inks have significantly reduced the cost of QD film fabrication.[37,50]

Extensive theoretical design and experimental device fabrication have been conducted by researchers regarding the tandem structure of perovskite/QD. The device parameters of reported perovskite/QD tandem solar cells are shown in Tables 4 and 5. Karani *et al.* (2018) predicted, through theoretical calculations considering inter-subcell radiation coupling, that a perovskite (1.55 eV)/PbS QD (1.0 eV) tandem structure could achieve an impressive PCE of 43%.[2] This study proposed a cost-effective, all-solution-based fabrication method, providing theoretical guidance for the design of perovskite/QD tandem cells. Although their initial prototype cell exhibited a modest efficiency of only 1.01%, it validated the voltage stacking effect of tandem cells. The subpar efficiency can be attributed to the combination of suboptimal subcell current matching and the less-than-ideal recombination layer. In the same year, Zhang *et al.* achieved efficient monolithic tandem solar cells composed of PbS and perovskite through all-solution processing.[25] They accomplished perfect voltage stacking and achieved a remarkable PCE of up to 11.03% by developing a solution-processed recombination layer of n-PEDOT/SnO_2 NPs and carefully adjusting the thickness of the subcells to match the current density (Fig. 5(c)–(e)). However, the proposed cell

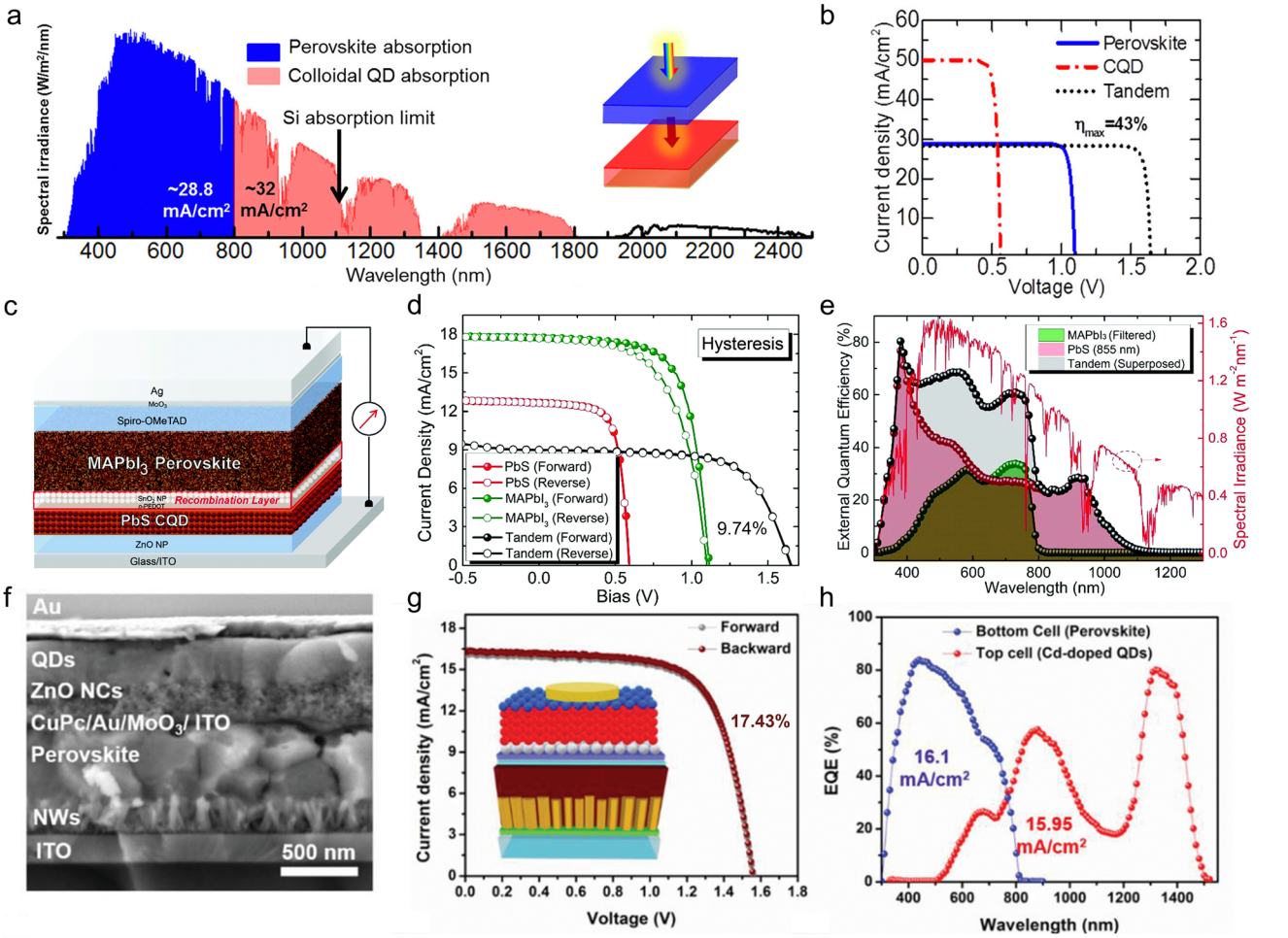

Fig. 5 (a) Solar spectrum (AM1.5 global) showing the limit of photocurrent generation by a typical perovskite solar cell with a bandgap of 1.55 eV, and the lower-energy photons that could be captured by low-bandgap CQDs ($E_g \geq 20.65$ eV).[2] (b) Theoretical J–V curves derived from the detailed balance model for ideal individual and tandem cells.[2] Reprinted with permission. Copyright 2022 American Chemical Society. (c) Device structure, (d) J–V and (e) EQE curves of the first realized high-efficiency 2T perovskite/QD tandem solar cell.[25] Reprinted with permission. Copyright 2018 Royal Society of Chemistry. (f) Device structure, (g) J–V and (h) EQE curves of the current most efficient 2T perovskite/QD tandem solar cell.[30] Reprinted with permission. Copyright 2021 Wiley-VCH GmbH.

Table 4 Summary of 2T perovskite/QD tandem solar cells

Sub-cells	E_g [eV]	Absorbers	CRL	V_{OC} [V]	J_{SC} [mA cm^{-2}]	FF [%]	PCE [%]	Ref.
Front cell	1.55	$MAPbI_3$	MoO_X/Au/ZnO	0.98	5	20	1.01	2
Back cell	1.21	PbS						
Front cell	1.45	PbS	n-PEDOT/SnO_2 NPs	1.66	8.91	74.6	11.03	25
Back cell	1.5	$MAPbI_3$						
Front cell	1.55	$Cs_{0.05}FA_{0.8}MA_{0.15}PbI_{2.55}Br_{0.45}$	Au/MoO_3/ITO	1.55	16.3	69	17.1	30
Back cell	0.92	PbS						

structure, with PbS QDs as the front cell, may result in increased energy losses.

In 2021, Tavakoli *et al.* fabricated perovskite/PbS QD tandem solar cells with perovskite as the front cell and QD as the rear cell.[30] They addressed the chemical instability issue at the ZnO/perovskite interface by employing SnO_2 passivated ZnO nanowire electron transport layers deposited *via* atomic layer deposition. Additionally, they replaced the commonly used 2,2,7,7-tetrakis(*N*,*N*-di-4-methoxyphenylamino)-9,9-spirobifluorene (spiro-OMeTAD) hole transport layer in perovskite with copper(II) phthalocyanine (CuPC), resulting in a reduced optimal thickness of the perovskite layer, enhanced stability of the tandem device, and reduced parasitic absorption caused by spiro doping. By combining the PbS QD rear cell passivated with $CdCl_2$ with optimized thickness and current matching, the efficiency of the monolithic 2T perovskite/PbS QD tandem solar cells reached 17.1%, marking the highest efficiency reported for monolithic 2T tandem structures based on PbS QDs (Fig. 5(f)–(h)).

Table 5 Summary of 4T perovskite/QD tandem solar cells

Sub-cells	E_g [eV]	Absorbers	V_{OC} [V]	J_{SC} [mA cm^{-2}]	FF [%]	PCE [%]	Total PCE [%]	Ref.
Semi-transparent front cell	1.63	$Cs_{0.05}MA_{0.10}FA_{0.85}PbI_{0.85}Br_{0.15}$	1.07	21.03	79.56	17.6	20.2	72
Filtered back cell	1.15	PbS	0.58	7.13	65.2	2.6		
Semi-transparent front cell	1.63	$Cs_{0.05}FA_{0.81}MA_{0.14}PbI_{2.55}Br_{0.45}$	1.12	22.3	77.7	19	24	73
Filtered back cell	1.2	PbS/IEICO-4F	0.62	12.2	66	5		
Semi-transparent front cell	1.55	$MAPbI_3$	1.05	21.5	76.9	17.4	18.9	74
Filtered back cell	1.13	PbS	0.52	4.83	61.1	1.5		
Semi-transparent front cell	1.55	$Cs_{0.05}FA_{0.8}MA_{0.15}PbI_{2.55}Br_{0.45}$	1.15	20.9	77	18.3	21.1	30
Filtered back cell	0.92	Cd-doped PbS	0.38	11.7	63	2.8		
Semi-transparent front cell	1.63	Perovskite	1.12	22.12	74.8	18.5	22.07	75
Filtered back cell	1.0	PbS	0.48	12.62	59.1	3.6		

Since fabricating 2T tandem devices is a significant challenge, particularly in the case of perovskite/PbS tandem devices, researchers have also attempted a simpler approach of mechanically connecting two subcells to prepare 4T tandem solar cells. In 2019, Manekkathodi *et al.* reported on a 4T tandem solar cell configuration with perovskite as the front cell and QDs as the rear cell.[72] The semi-transparent perovskite front cell employed a transparent conductive electrode consisting of MoO_3/Au/Ag/MoO_3 to enhance infrared transmittance. The structural improvements, designed based on the optical admittance diagram's zero-reflection condition, resulted in a 25% increase in infrared transmittance compared to the reference device. The fabricated 4T perovskite/QD tandem solar cell ultimately achieved a PCE exceeding 20%. In 2020, Chen *et al.* employed a technique called ''boosted solvent extraction'' to increase the thickness of the perovskite layer while maintaining its smooth and uniform morphology, thereby enhancing the absorption of near-infrared light in the semi-transparent cell.[73] Additionally, the addition of the Lewis base urea reduced the trap density in the perovskite layer and improved the electron diffusion length, resulting in reduced current losses. Furthermore, the combination of PbS:IEICO-4F as an organic-hybrid rear cell improved the near-infrared response. The fabricated 4T tandem cell exhibited efficient photon harvesting capabilities, achieving a J_{SC} of 34.5 mA cm^{-2} and a PCE of 24%. In the same year, Lee *et al.* introduced aromatic ligands to create weakly polar orthogonal QD inks. They successfully fabricated QD hole transport layers in a single-step spin-coating process, thus avoiding potential damage to the underlying active materials that might be caused by the solid-state ligand exchange steps, and also reduced the number of trap states in the hole transport layer. By layering the QD sub-cell, which featured a benzoic acid (BA) ligand-based hole transport layer, with a semi-transparent perovskite front cell, they achieved a J_{SC} of 34.7 mA cm^{-2} and a PCE of 22%.[75] In 2021, Andruszkiewicz *et al.* modified the insulating separation layer between the perovskite and PbS QD subcells in the 4T tandem solar cell structure.[74] They added a Surlyn layer onto the semi-transparent thin gold electrode at the top of the $MAPbI_3$ front cell to replace the air gap between the subcells. This modification resulted in a reduction of optical losses such as absorption and reflection at the interface, while simultaneously enhancing infrared light transmittance. Compared to the devices without the surlyn layer, the addition of the surlyn layer elevated the PCE of the devices by approximately 13% and increased J_{SC} by approximately 8%.

The perovskite/QD tandem architecture represents a significant approach to enhancing the PCE of perovskite solar cells. Currently, research on the perovskite/QD tandem structure remains relatively limited. The fabrication of efficient monolithic 2T tandem devices still poses significant technological challenges, with limited progress achieved thus far. One of the challenges is the compatibility of the fabrication process, where the ideal structure is to incorporate infrared QD solar cells onto perovskite. However, perovskite is very fragile, and it is easy to be damaged during the fabrication of top QD cells. In the future, systematic research on the surface chemistry of QD is needed to develop new solvents and fabrication processes that can be compatible with the underlying perovskite. Additionally, there has been rapid development in the p–i–n structure of perovskite, which is more suitable for fabricating layered devices. However, the research on high-efficiency p–i–n structured QD solar cells is still in its infancy, with only a handful of studies reported.[76–79] Its highest PCE is only 9.7%,[78] far behind the maximum PCE of n–i–p (15.45%).[80] Future development should focus on finding highly efficient p-type hole transport materials compatible with ITO, along with improving electrode materials and interface layer designs, to enhance the efficiency and stability of solar cells.

Conclusions

Tandem solar cells based on QDs are an emerging solar cell technology that holds potential to surpass the PCE limits of single-junction solar cells. This paper comprehensively presents the latest research advancements in this technology. We initially introduce the fundamental architecture and working principles of tandem solar cells. Subsequently, we delve into the research progress of three different types of tandem solar cells: QD/QD, organic/QD, and perovskite/QD. By reviewing these research advancements, our aim is to provide a reference for further enhancing the efficiency of QD-based solar cells. Furthermore, we propose several suggestions for future development in this direction:

(1) Currently, a critical factor impeding the advancement of tandem solar cells based on QDs is the suboptimal PCE of single-junction QD photovoltaic devices. QD materials, due to

Table 6 Infrared QD solar cell performances measured with a long-pass filter

Solar illumination	V_{OC} (V)	J_{SC} (mA cm^{-2})	FF	PCE (%)	Year	Ref.
1100 nm filter	0.40	3.0	0.61	0.8	2015	89
	0.29	2.4	0.58	0.4	2016	90
	0.44	2.7	0.62	0.7	2017	91
	0.43	3.2	0.67	0.9	2018	92
	0.40	3.70	0.65	0.94	2018	81
	0.41	4.1	0.64	1.1	2018	93
	0.39	3.84	0.66	0.99	2018	94
	0.43	3.2	0.65	0.9	2019	82
	0.37	4.1	0.64	0.96	2019	95
	0.39	4.3	0.64	1.1	2019	32
	0.47	4.4	0.59	1.2	2019	96
	0.43	5.6	0.56	1.34	2019	64
	0.43	5.5	0.58	1.37	2020	97
	0.30	9.81	0.53	1.57	2020	98
	0.438	5.34	0.61	1.43	2020	75
	0.347	6.78	0.556	1.31	2021	99
	0.347	6.38	0.56	1.24	2021	83
	0.418	4.78	0.61	1.23	2022	84
	0.42	4.6	0.65	1.25	2022	100
	0.395	5.56	0.59	1.3	2023	101
	0.425	4.99	0.67	1.42	2023	85
	0.40	6.02	0.60	1.44	2023	54
800 nm filter	0.459	13.42	0.63	3.90	2021	84
	0.439	15.77	0.61	4.2	2020	32
	0.47	15.64	0.65	4.73	2023	102
	0.469	15.14	0.68	4.84	2023	85

their large specific surface area and high surface defect state concentration, result in significant voltage losses. Particularly for narrow-bandgap PbX QDs, the increase of non-polar (100) facets poses a more challenging surface passivation. Hence, it necessitates further exploration of surface passivation techniques for large-sized narrow-bandgap PbX QDs.[81–86] Recently, researchers have incorporated long-pass filters with wavelengths of 800 nm or 1100 nm between a solar simulator and the narrow-bandgap QD devices to simulate perovskite/QD and silicon/QD 4T tandem solar cells (Table 6). This simplified method enables researchers to focus primarily on studying the optoelectronic performance of QDs in the infrared spectrum. It serves as an effective means to accelerate the research progress in this field. Upon effectively enhancing the efficiency of single-junction PbX QD cells, the efficiency of the tandem can be naturally improved as well.

(2) The recently developed methods for synthesizing QD semiconductor inks (liquid-phase ligand exchange and direct synthesis methods) exhibit significant advantages over traditional solid-phase ligand exchange in terms of surface passivation and simplification of device fabrication processes.[37,87,88] However, the colloidal stability of large-sized PbX QD semiconductor inks is poor, which restricts the device performance of high-efficiency single-junction infrared QD cells. This issue will become even more severe in the future during the fabrication of large-area devices. Furthermore, the dispersal solutions of PbX QD semiconductor inks currently consist mostly of highly polar solvents (such as butylamine and DMF), which often cause damage to the underlying subcells in the process of tandem device fabrication. This is also one of the crucial factors limiting the preparation of high-efficiency tandem devices. Therefore, a detailed investigation of the dispersion mechanism of QD semiconductor inks and the development of a versatile dispersion solvent system compatible with the fabrication of tandem solar cells are required.

(3) The current infrared QD material system is excessively monotonous and plagued by the toxicity issue of heavy metal Pb, which likewise hampers its prospective large-scale applications. The recently emerging $AgBiS_2$ QDs, green and environmentally friendly materials, exhibit an exceedingly high absorption coefficient and have garnered remarkable attention.[103–108] Their single-junction devices have already achieved PCE approaching 10%. However, compared to PbX QDs, their bandgap is wide, rendering them non-ideal for the fabrication of tandem devices. Therefore, in the future, exploration can be undertaken with other I–V–VI class QD materials, such as $AgBiSe_2$, which may possess narrower bandgaps. This holds promise in realizing efficient and stable infrared QD tandem devices, with potential applications in the realm of biotechnology.

In conclusion, tandem solar cells based on QDs represent a tremendously promising new frontier in solar energy technology. Despite the numerous challenges currently being faced, we hold the belief that through the continual development and refinement of novel materials and innovative processes, this type of solar cell holds potential in realizing an efficient, cost-effective, and environmentally friendly energy supply in the future. We eagerly anticipate witnessing further innovations and breakthroughs in future research endeavours.

Conflicts of interest

The authors declare no competing financial interest.

Acknowledgements

This work was supported by the National Natural Science Foundation of China (grant no. 52372215, 52002260 and 92163114), the Natural Science Foundation of Jiangsu Province of China (BK20230504), the Special Fund for the ''Dual Carbon'' Science and Technology Innovation of Jiangsu province (Industrial Prospect and Key Technology Research program) (BE2022023, BE2022021), the Natural Science Foundation of the Jiangsu Higher Education Institutions of China (21KJA430004), and the Gusu Innovation and Entrepreneurship Leading Talent Program (ZXL2022451). This work was supported by the China Postdoctoral Science Foundation (no. 2023M732523) and the Suzhou Key Laboratory of Functional Nano & Soft Materials, Collaborative Innovation Center of Suzhou Nano Science & Technology, the 111 Project.

Notes and references

1 S. Wu, M. Liu and A. K. Y. Jen, Prospects and challenges for perovskite-organic tandem solar cells, *Joule*, 2023, **7**, 484–502.

2 A. Karani, L. Yang, S. Bai, M. H. Futscher, H. J. Snaith, B. Ehrler, N. C. Greenham and D. Di, Perovskite/colloidal quantum dot tandem solar cells: theoretical modeling and monolithic structure, *ACS Energy Lett.*, 2018, **3**, 869–874.
3 J. J. Choi, W. N. Wenger, R. S. Hoffman, Y.-F. Lim, J. Luria, J. Jasieniak, J. A. Marohn and T. Hanrath, Solution-processed nanocrystal quantum dot tandem solar cells, *Adv. Mater.*, 2011, **23**, 3144–3148.
4 T. Kim, Y. Gao, H. Hu, B. Yan, Z. Ning, L. K. Jagadamma, K. Zhao, A. R. Kirmani, J. Eid, M. M. Adachi, E. H. Sargent, P. M. Beaujuge and A. Amassian, Hybrid tandem solar cells with depleted-heterojunction quantum dot and polymer bulk heterojunction subcells, *Nano Energy*, 2015, **17**, 196–205.
5 M. A. Green and S. P. Bremner, Energy conversion approaches and materials for high-efficiency photovoltaics, *Nat. Mater.*, 2017, **16**, 23–34.
6 A. Polman, M. Knight, E. C. Garnett, B. Ehrler and W. C. Sinke, Photovoltaic materials: present efficiencies and future challenges, *Science*, 2016, **352**, aad4424.
7 Z. Song, C. Chen, C. Li, R. A. Awni, D. Zhao and Y. Yan, Wide-bandgap, low-bandgap, and tandem perovskite solar cells, *Semicond. Sci. Technol.*, 2019, **34**, 093001.
8 R. W. Crisp, G. F. Pach, J. M. Kurley, R. M. France, M. O. Reese, S. U. Nanayakkara, B. A. MacLeod, D. V. Talapin, M. C. Beard and J. M. Luther, Tandem solar cells from solution-processed CdTe and PbS quantum dots ssing a ZnTe–ZnO tunnel junction, *Nano Lett.*, 2017, **17**, 1020–1027.
9 W. Shockley and H. J. Queisser, Detailed balance limit of efficiency of p–n junction solar cells, *J. Appl. Phys.*, 1961, **32**, 510–519.
10 J. Tong, X. Yang, Y. Xu, W. Li, J. Tang, H. Song and Y. Zhou, Efficient top-illuminated organic-quantum dots hybrid tandem solar cells with complementary absorption, *ACS Photonics*, 2017, **4**, 1172–1177.
11 X. Wang, G. I. Koleilat, J. Tang, H. Liu, I. J. Kramer, R. Debnath, L. Brzozowski, D. A. R. Barkhouse, L. Levina, S. Hoogland and E. H. Sargent, Tandem colloidal quantum dot solar cells employing a graded recombination layer, *Nat. Photonics*, 2011, **5**, 480–484.
12 Best research cell efficiencies (NREL, accessed on 20230901), **https://www.nrel.gov/pv/cell-efficiency.htm**).
13 F. Fu, J. Li, T. C.-J. Yang, H. Liang, A. Faes, Q. Jeangros, C. Ballif and Y. Hou, Monolithic perovskite-silicon tandem solar cells: from the lab to fab?, *Adv. Mater.*, 2022, **34**, 2106540.
14 L. Duan, D. Walter, N. Chang, J. Bullock, D. Kang, S. P. Phang, K. Weber, T. White, D. Macdonald, K. Catchpole and H. Shen, Stability challenges for the commercialization of perovskite–silicon tandem solar cells, *Nat. Rev. Mater.*, 2023, **8**, 261–281.
15 D. P. McMeekin, S. Mahesh, N. K. Noel, M. T. Klug, J. Lim, J. H. Warby, J. M. Ball, L. M. Herz, M. B. Johnston and H. J. Snaith, Solution-processed all-perovskite multi-junction solar cells, *Joule*, 2019, **3**, 387–401.
16 K. O. Brinkmann, T. Becker, F. Zimmermann, C. Kreusel, T. Gahlmann, M. Theisen, T. Haeger, S. Olthof, C. Tuckmantel, M. Gunster, T. Maschwitz, F. Gobelsmann, C. Koch, D. Hertel, P. Caprioglio, F. Pena-Camargo, L. Perdigon-Toro, A. Al-Ashouri, L. Merten, A. Hinderhofer, L. Gomell, S. Zhang, F. Schreiber, S. Albrecht, K. Meerholz, D. Neher, M. Stolterfoht and T. Riedl, Perovskite-organic tandem solar cells with indium oxide interconnect, *Nature*, 2022, **604**, 280–286.
17 H. Chen, A. Maxwell, C. Li, S. Teale, B. Chen, T. Zhu, E. Ugur, G. Harrison, L. Grater, J. Wang, Z. Wang, L. Zeng, S. M. Park, L. Chen, P. Serles, R. A. Awni, B. Subedi, X. Zheng, C. Xiao, N. J. Podraza, T. Filleter, C. Liu, Y. Yang, J. M. Luther, S. De Wolf, M. G. Kanatzidis, Y. Yan and E. H. Sargent, Regulating surface potential maximizes voltage in all-perovskite tandems, *Nature*, 2023, **613**, 676–681.
18 R. He, W. Wang, Z. Yi, F. Lang, C. Chen, J. Luo, J. Zhu, J. Thiesbrummel, S. Shah, K. Wei, Y. Luo, C. Wang, H. Lai, H. Huang, J. Zhou, B. Zou, X. Yin, S. Ren, X. Hao, L. Wu, J. Zhang, J. Zhang, M. Stolterfoht, F. Fu, W. Tang and D. Zhao, Improving interface quality for 1-cm^2 all-perovskite tandem solar cells, *Nature*, 2023, **618**, 80–86.
19 R. Lin, Y. Wang, Q. Lu, B. Tang, J. Li, H. Gao, Y. Gao, H. Li, C. Ding, J. Wen, P. Wu, C. Liu, S. Zhao, K. Xiao, Z. Liu, C. Ma, Y. Deng, L. Li, F. Fan and H. Tan, All-perovskite tandem solar cells with 3D/3D bilayer perovskite heterojunction, *Nature*, 2023, **620**, 994–1000.
20 R. Lin, J. Xu, M. Wei, Y. Wang, Z. Qin, Z. Liu, J. Wu, K. Xiao, B. Chen, S. M. Park, G. Chen, H. R. Atapattu, K. R. Graham, J. Xu, J. Zhu, L. Li, C. Zhang, E. H. Sargent and H. Tan, All-perovskite tandem solar cells with improved grain surface passivation, *Nature*, 2022, **603**, 73–78.
21 W. Chen, Y. Zhu, J. Xiu, G. Chen, H. Liang, S. Liu, H. Xue, E. Birgersson, J. W. Ho, X. Qin, J. Lin, R. Ma, T. Liu, Y. He, A. M.-C. Ng, X. Guo, Z. He, H. Yan, A. B. Djurišić and Y. Hou, Monolithic perovskite/organic tandem solar cells with 23.6% efficiency enabled by reduced voltage losses and optimized interconnecting layer, *Nat. Energy*, 2022, **7**, 229–237.
22 R. Wang, T. Huang, J. Xue, J. Tong, K. Zhu and Y. Yang, Prospects for metal halide perovskite-based tandem solar cells, *Nat. Photonics*, 2021, **15**, 411–425.
23 K. Xiao, Y.-H. Lin, M. Zhang, R. D. J. Oliver, X. Wang, Z. Liu, X. Luo, J. Li, D. Lai, H. Luo, R. Lin, J. Xu, Y. Hou, H. J. Snaith and H. Tan, Scalable processing for realizing 21.7%-efficient all-perovskite tandem solar modules, *Science*, 2022, **376**, 762–767.
24 I. Moreels, Y. Justo, B. De Geyter, K. Haustraete, J. C. Martins and Z. Hens, Size-Tunable, Bright, and Stable PbS Quantum Dots: A Surface Chemistry Study, *ACS Nano*, 2011, **5**, 2004–2012.
25 Y. Zhang, M. Gu, N. Li, Y. Xu, X. Ling, Y. Wang, S. Zhou, F. Li, F. Yang, K. Ji, J. Yuan and W. Ma, Realizing solution-processed monolithic PbS QDs/perovskite tandem solar cells with high UV stability, *J. Mater. Chem. A*, 2018, **6**, 24693–24701.

26 G. Shi, Y. Wang, Z. Liu, L. Han, J. Liu, Y. Wang, K. Lu, S. Chen, X. Ling, Y. Li, S. Cheng and W. Ma, Stable and highly efficient PbS quantum dot tandem solar cells employing a rationally designed recombination layer, *Adv. Energy Mater.*, 2017, **7**, 1602667.
27 H. I. Kim, S. W. Baek, M. J. Choi, B. Chen, O. Ouellette, K. Choi, B. Scheffel, H. Choi, M. Biondi, S. Hoogland, F. P. García De Arquer, T. Park and E. H. Sargent, Monolithic organic/colloidal quantum dot hybrid tandem solar cells *via* buffer engineering, *Adv. Mater.*, 2020, **32**, 2004657.
28 I. Moreels, K. Lambert, D. Smeets, D. De Muynck, T. Nollet, J. C. Martins, F. Vanhaecke, A. Vantomme, C. Delerue, G. Allan and Z. Hens, Size-dependent optical properties of colloidal PbS quantum dots, *ACS Nano*, 2009, **3**, 3023–3030.
29 G. E. Eperon, M. T. Hörantner and H. J. Snaith, Metal halide perovskite tandem and multiple-junction photovoltaics, *Nat. Rev. Chem.*, 2017, **1**, 1–18.
30 M. M. Tavakoli, H. T. Dastjerdi, P. Yadav, D. Prochowicz, H. Si and R. Tavakoli, Ambient stable and efficient monolithic tandem perovskite/PbS quantum dots solar cells *via* surface passivation and light management strategies, *Adv. Funct. Mater.*, 2021, **31**, 2010623.
31 Y. Bi, S. Pradhan, M. Z. Akgul, S. Gupta, A. Stavrinadis, J. Wang and G. Konstantatos, Colloidal quantum dot tandem solar cells using chemical vapor deposited graphene as an atomically thin intermediate recombination layer, *ACS Energy Lett.*, 2018, **3**, 1753–1759.
32 Y. Xia, S. Liu, K. Wang, X. Yang, L. Lian, Z. Zhang, J. He, G. Liang, S. Wang, M. Tan, H. Song, D. Zhang, J. Gao, J. Tang, M. C. Beard and J. Zhang, Cation-exchange synthesis of highly monodisperse PbS quantum dots from ZnS nanorods for efficient infrared solar cells, *Adv. Funct. Mater.*, 2020, **30**, 1907379.
33 Y. Gao, J. Zheng, W. Chen, L. Yuan, Z. L. Teh, J. Yang, X. Cui, G. Conibeer, R. Patterson and S. Huang, Enhancing PbS colloidal quantum dot tandem solar cell performance by graded band alignment, *J. Phys. Chem. Lett.*, 2019, **10**, 5729–5734.
34 Q. Zhao, R. Han, A. R. Marshall, S. Wang, B. M. Wieliczka, J. Ni, J. Zhang, J. Yuan, J. M. Luther, A. Hazarika and G. R. Li, Colloidal quantum dot solar cells: progressive deposition techniques and future prospects on large-area fabrication, *Adv. Mater.*, 2022, **34**, e2107888.
35 H. Lee, H. J. Song, M. Shim and C. Lee, Towards the commercialization of colloidal quantum dot solar cells: perspectives on device structures and manufacturing, *Energy Environ. Sci.*, 2020, **13**, 404–431.
36 Y. Liu, G. Shi, Z. Liu and W. Ma, Toward printable solar cells based on PbX colloidal quantum dot inks, *Nanoscale Horiz.*, 2021, **6**, 8–23.
37 Y. Wang, Z. Liu, N. Huo, F. Li, M. Gu, X. Ling, Y. Zhang, K. Lu, L. Han, H. Fang, A. G. Shulga, Y. Xue, S. Zhou, F. Yang, X. Tang, J. Zheng, M. Antonietta Loi, G. Konstantatos and W. Ma, Room-temperature direct synthesis of semi-conductive PbS nanocrystal inks for optoelectronic applications, *Nat. Commun.*, 2019, **10**, 5136.
38 M. C. Weidman, M. E. Beck, R. S. Hoffman, F. Prins and W. A. Tisdale, Monodisperse, air-stable PbS nanocrystals *via* precursor stoichiometry control, *ACS Nano*, 2014, **8**, 6363–6371.
39 C. Dong, S. Liu, N. Barange, J. Lee, T. Pardue, X. Yi, S. Yin and F. So, Long-wavelength lead sulfide quantum dots sensing up to 2600 nm for short-wavelength infrared photodetectors, *ACS Appl. Mater. Interfaces*, 2019, **11**, 44451–44457.
40 M. P. Campos, M. P. Hendricks, A. N. Beecher, W. Walravens, R. A. Swain, G. T. Cleveland, Z. Hens, M. Y. Sfeir and J. S. Owen, A library of selenourea precursors to PbSe nanocrystals with size distributions near the homogeneous limit, *J. Am. Chem. Soc.*, 2017, **139**, 2296–2305.
41 J. M. Pietryga, R. D. Schaller, D. Werder, M. H. Stewart, V. I. Klimov and J. A. Hollingsworth, Pushing the band gap envelope: mid-infrared emitting colloidal PbSe quantum dots, *J. Am. Chem. Soc.*, 2004, **126**, 11752–11753.
42 M. P. Hendricks, M. P. Campos, G. T. Cleveland, I. Jen-La Plante and J. S. Owen, A tunable library of substituted thiourea precursors to metal sulfide nanocrystals, *Science*, 2015, **348**, 1226–1230.
43 Z. Ning, D. Zhitomirsky, V. Adinolfi, B. Sutherland, J. Xu, O. Voznyy, P. Maraghechi, X. Lan, S. Hoogland, Y. Ren and E. H. Sargent, Graded doping for enhanced colloidal quantum dot photovoltaics, *Adv. Mater.*, 2013, **25**, 1719–1723.
44 R. Wang, Y. Shang, P. Kanjanaboos, W. Zhou, Z. Ning and E. H. Sargent, Colloidal quantum dot ligand engineering for high performance solar cells, *Energy Environ. Sci.*, 2016, **9**, 1130–1143.
45 D. Zhitomirsky, M. Furukawa, J. Tang, P. Stadler, S. Hoogland, O. Voznyy, H. Liu and E. H. Sargent, N-type colloidal-quantum-dot solids for photovoltaics, *Adv. Mater.*, 2012, **24**, 6181–6185.
46 O. Voznyy, D. Zhitomirsky, P. Stadler, Z. Ning, S. Hoogland and E. H. Sargent, A charge-orbital balance picture of doping in colloidal quantum dot solids, *ACS Nano*, 2012, **6**, 8448–8455.
47 P. R. Brown, D. Kim, R. R. Lunt, N. Zhao, M. G. Bawendi, J. C. Grossman and V. Bulovic, Energy level modification in lead sulfide quantum dot thin films through ligand exchange, *ACS Nano*, 2014, **8**, 5863–5872.
48 H. Wang, M. Desbordes, Y. Xiao, T. Kubo, K. Tada, T. Bessho, J. Nakazaki and H. Segawa, Highly stable interdigitated PbS quantum dot and ZnO nanowire solar cells with an automatically embedded electron-blocking layer, *ACS Appl. Energy Mater.*, 2021, **4**, 5918–5926.
49 C. H. Chuang, P. R. Brown, V. Bulovic and M. G. Bawendi, Improved performance and stability in quantum dot solar cells through band alignment engineering, *Nat. Mater.*, 2014, **13**, 796–801.
50 Y. Liu, F. Li, G. Shi, Z. Liu, X. Lin, Y. Shi, Y. Chen, X. Meng, Y. Lv, W. Deng, X. Pan and W. Ma, PbSe quantum dot solar cells based on directly synthesized semiconductive inks, *ACS Energy Lett.*, 2020, **5**, 3797–3803.
51 S. Fang, J. Huang, R. Tao, Q. Wei, X. Ding, S. Yajima, Z. Chen, W. Zhu, C. Liu, Y. Li, N. Yin, L. Song, Y. Liu,

G. Shi, H. Wu, Y. Gao, X. Wen, Q. Chen, Q. Shen, Y. Li, Z. Liu, Y. Li and W. Ma, Open-shell diradical-sensitized electron transport layer for high-performance colloidal quantum dot solar cells, *Adv. Mater.*, 2023, **35**, e2212184.

52 Y. Liu, H. Wu, G. Shi, Y. Li, Y. Gao, S. Fang, H. Tang, W. Chen, T. Ma, I. Khan, K. Wang, C. Wang, X. Li, Q. Shen, Z. Liu and W. Ma, Merging passivation in synthesis enabling the lowest open-circuit voltage loss for PbS quantum dot solar cells, *Adv. Mater.*, 2023, **35**, e2207293.

53 F. Li, Y. Liu, G. Shi, W. Chen, R. Guo, D. Liu, Y. Zhang, Y. Wang, X. Meng, X. Zhang, Y. Lv, W. Deng, Q. Zhang, Y. Shi, Y. Chen, K. Wang, Q. Shen, Z. Liu, P. Müller-Buschbaum and W. Ma, Matrix manipulation of directly-synthesized PbS quantum dot inks enabled by coordination engineering, *Adv. Funct. Mater.*, 2021, **31**, 2104457.

54 Y. Liu, Y. Gao, Q. Yang, G. Xu, X. Zhou, G. Shi, X. Lyu, H. Wu, J. Liu, S. Fang, M. I. Ullah, L. Song, K. Lu, M. Cao, Q. Zhang, T. Li, J. Xu, S. Wang, Z. Liu and W. Ma, Breaking the size limitation of directly-synthesized PbS quantum dot inks toward efficient short-wavelength infrared optoelectronic applications, *Angew. Chem., Int. Ed.*, 2023, **62**, e202300396.

55 J. Liu, Z. Zhou, Y. Gao, Y. Wu, J. Wang, H. Li, Q. Wang, K. Zhou, K. Xian, Y. Chen, W. Zhao, F. Zhang, H. Yin, Y. Liu, K. Zhao, J. Yan and L. Ye, Polymer synergy for efficient hole transport in solar cells and photodetectors, *Energy Environ. Sci.*, 2023, **16**, 4474–4485.

56 X. Xu, Y. Li and Q. Peng, Recent advances toward highly efficient tandem organic solar cells, *Small Struct.*, 2020, **1**, 2000016.

57 M. Zhang and Z. Lin, Efficient interconnecting layers in monolithic all-perovskite tandem solar cells, *Energy Environ. Sci.*, 2022, **15**, 3152–3170.

58 J. Werner, B. Niesen and C. Ballif, Perovskite/silicon tandem solar cells: marriage of convenience or true love story? – an overview, *Adv. Mater. Interfaces*, 2018, **5**, 1700731.

59 Z. Zhu, K. Mao and J. Xu, Perovskite tandem solar cells with improved efficiency and stability, *J. Energy Chem.*, 2021, **58**, 219–232.

60 M. Boccard and C. Ballif, Influence of the subcell properties on the fill factor of two-terminal perovskite–silicon tandem solar cells, *ACS Energy Lett.*, 2020, **5**, 1077–1082.

61 M. A. Hines and G. D. Scholes, Colloidal PbS nanocrystals with size-tunable near-infrared emission: observation of post-synthesis self-narrowing of the particle size distribution, *Adv. Mater.*, 2003, **15**, 1844–1849.

62 H. Choi, J. H. Ko, Y. H. Kim and S. Jeong, Steric-hindrance-driven shape transition in PbS quantum dots: understanding size-dependent stability, *J. Am. Chem. Soc.*, 2013, **135**, 5278–5281.

63 H. Lu, G. M. Carroll, N. R. Neale and M. C. Beard, Infrared quantum dots: progress, challenges, and opportunities, *ACS Nano*, 2019, **13**, 939–953.

64 S.-W. Baek, P. Molet, M.-J. Choi, M. Biondi, O. Ouellette, J. Fan, S. Hoogland, F. P. García de Arquer, A. Mihi and E. H. Sargent, Nanostructured back reflectors for efficient colloidal quantum-dot infrared optoelectronics, *Adv. Mater.*, 2019, **31**, 1901745.

65 L. Hu, Y. Wang, S. B. Shivarudraiah, J. Yuan, X. Guan, X. Geng, A. Younis, Y. Hu, S. Huang, T. Wu and J. E. Halpert, Quantum-dot tandem solar cells based on a solution-processed nanoparticle intermediate layer, *ACS Appl. Mater. Interfaces*, 2020, **12**, 2313–2318.

66 M. J. Speirs, B. G. H. M. Groeneveld, L. Protesescu, C. Piliego, M. V. Kovalenko and M. A. Loi, Hybrid inorganic–organic tandem solar cells for broad absorption of the solar spectrum, *Phys. Chem. Chem. Phys.*, 2014, **16**, 7672–7676.

67 H. Aqoma, R. Azmi, S.-H. Oh and S.-Y. Jang, Solution-processed colloidal quantum dot/organic hybrid tandem photovoltaic devices with 8.3% efficiency, *Nano Energy*, 2017, **31**, 403–409.

68 T. Kim, E. Palmiano, R.-Z. Liang, H. Hu, B. Murali, A. R. Kirmani, Y. Firdaus, Y. Gao, A. Sheikh, M. Yuan, O. F. Mohammed, S. Hoogland, P. M. Beaujuge, E. H. Sargent and A. Amassian, Hybrid tandem quantum dot/organic photovoltaic cells with complementary near infrared absorption, *Appl. Phys. Lett.*, 2017, **110**, 223903.

69 H. Aqoma, I. F. Imran, M. A. Mubarok, W. T. Hadmojo, Y. R. Do and S. Y. Jang, Efficient hybrid tandem solar cells based on optical reinforcement of colloidal quantum dots with organic bulk heterojunctions, *Adv. Energy Mater.*, 2020, **10**, 1903294.

70 Y.-L. Li, P.-N. Yeh, S. Sharma and S.-A. Chen, Promotion of performances of quantum dot solar cell and its tandem solar cell with low bandgap polymer (PTB7-Th):$PC_{71}BM$ by water vapor treatment on quantum dot layer on its surface, *J. Mater. Chem. A*, 2017, **5**, 21528–21535.

71 T. Kim, Y. Firdaus, A. R. Kirmani, R.-Z. Liang, H. Hu, M. Liu, A. El Labban, S. Hoogland, P. M. Beaujuge, E. H. Sargent and A. Amassian, Hybrid tandem quantum dot/organic solar cells with enhanced photocurrent and efficiency *via* ink and interlayer engineering, *ACS Energy Lett.*, 2018, **3**, 1307–1314.

72 A. Manekkathodi, B. Chen, J. Kim, S.-W. Baek, B. Scheffel, Y. Hou, O. Ouellette, M. I. Saidaminov, O. Voznyy, V. E. Madhavan, A. Belaidi, S. Ashhab and E. Sargent, Solution-processed perovskite-colloidal quantum dot tandem solar cells for photon collection beyond 1000 nm, *J. Mater. Chem. A*, 2019, **7**, 26020–26028.

73 B. Chen, S.-W. Baek, Y. Hou, E. Aydin, M. De Bastiani, B. Scheffel, A. Proppe, Z. Huang, M. Wei, Y.-K. Wang, E.-H. Jung, T. G. Allen, E. Van Kerschaver, F. P. García De Arquer, M. I. Saidaminov, S. Hoogland, S. De Wolf and E. H. Sargent, Enhanced optical path and electron diffusion length enable high-efficiency perovskite tandems, *Nat. Commun.*, 2020, **11**, 1257.

74 A. Andruszkiewicz, X. Zhang, M. B. Johansson, L. Yuan and E. M. J. Johansson, Perovskite and quantum dot tandem solar cells with interlayer modification for improved optical semitransparency and stability, *Nanoscale*, 2021, **13**, 6234–6240.

75 S. Lee, M.-J. Choi, G. Sharma, M. Biondi, B. Chen, S.-W. Baek, A. M. Najarian, M. Vafaie, J. Wicks, L. K. Sagar, S. Hoogland, F. P. G. De Arquer, O. Voznyy and E. H. Sargent, Orthogonal colloidal quantum dot inks enable efficient multilayer optoelectronic devices, *Nat. Commun.*, 2020, **11**, 4814.

76 K. Lu, Y. Wang, J. Yuan, Z. Cui, G. Shi, S. Shi, L. Han, S. Chen, Y. Zhang, X. Ling, Z. Liu, L. Chi, J. Fan and W. Ma, Efficient PbS quantum dot solar cells employing a conventional structure, *J. Mater. Chem. A*, 2017, **5**, 23960–23966.

77 M. M. Tavakoli, M. H. Gharahcheshmeh, N. Moody, M. G. Bawendi, K. K. Gleason and J. Kong, Efficient, flexible, and ultra-lightweight inverted PbS quantum dots solar cells on all-CVD-growth of parylene/graphene/oCVD PEDOT substrate with high power-per-weight, *Adv. Mater. Interfaces*, 2020, **7**, 2000498.

78 R. Wang, X. Wu, K. Xu, W. Zhou, Y. Shang, H. Tang, H. Chen and Z. Ning, Highly efficient inverted structural quantum dot solar cells, *Adv. Mater.*, 2018, **30**, 1704882.

79 V. M. Goossens, N. V. Sukharevska, D. N. Dirin, M. V. Kovalenko and M. A. Loi, Scalable fabrication of efficient p-n junction lead sulfide quantum dot solar cells, *Cell Rep. Phys. Sci.*, 2021, **2**, 100655.

80 C. Ding, D. Wang, D. Liu, H. Li, Y. Li, S. Hayase, T. Sogabe, T. Masuda, Y. Zhou, Y. Yao, Z. Zou, R. Wang and Q. Shen, Over 15% efficiency PbS quantum-dot solar cells by synergistic effects of three interface engineering: reducing nonradiative recombination and balancing charge carrier extraction, *Adv. Energy Mater.*, 2022, **12**, 2201676.

81 B. Sun, O. Ouellette, F. P. García de Arquer, O. Voznyy, Y. Kim, M. Wei, A. H. Proppe, M. I. Saidaminov, J. Xu, M. Liu, P. Li, J. Z. Fan, J. W. Jo, H. Tan, F. Tan, S. Hoogland, Z. H. Lu, S. O. Kelley and E. H. Sargent, Multibandgap quantum dot ensembles for solar-matched infrared energy harvesting, *Nat. Commun.*, 2018, **9**, 4003.

82 Y. Kim, F. Che, J. W. Jo, J. Choi, F. P. García de Arquer, O. Voznyy, B. Sun, J. Kim, M.-J. Choi, R. Quintero-Bermudez, F. Fan, C. S. Tan, E. Bladt, G. Walters, A. H. Proppe, C. Zou, H. Yuan, S. Bals, J. Hofkens, M. B. J. Roeffaers, S. Hoogland and E. H. Sargent, A facet-specific quantum dot passivation strategy for colloid management and efficient infrared photovoltaics, *Adv. Mater.*, 2019, **31**, 1805580.

83 S. Liu, C. Zhang, S. Li, Y. Xia, K. Wang, K. Xiong, H. Tang, L. Lian, X. Liu, M.-Y. Li, M. Tan, L. Gao, G. Niu, H. Liu, H. Song, D. Zhang, J. Gao, X. Lan, K. Wang, X. W. Sun, Y. Yang, J. Tang and J. Zhang, Efficient infrared solar cells employing quantum dot solids with strong inter-dot coupling and efficient passivation, *Adv. Funct. Mater.*, 2021, **31**, 2006864.

84 M. Li, S. Chen, X. Zhao, K. Xiong, B. Wang, U. A. Shah, L. Gao, X. Lan, J. Zhang, H.-Y. Hsu, J. Tang and H. Song, Matching charge extraction contact for infrared PbS colloidal quantum dot solar cells, *Small*, 2022, **18**, e2105495.

85 M. Li, X. Zhao, A. Zhang, B. Wang, Y. Yang, S. Xu, Q. Hu, G. Liang, Z. Xiao, L. Gao, J. Zhang, H.-Y. Hsu, H. Song and J. Tang, Organic ligand complementary passivation to Colloidal-quantum-dot surface enables efficient infrared solar cells, *Chem. Eng. J.*, 2023, **455**, 140961.

86 Y. Bi, S. Pradhan, S. Gupta, M. Z. Akgul, A. Stavrinadis and G. Konstantatos, Infrared solution-processed quantum dot solar cells reaching external quantum efficiency of 80% at 1.35 μm and J_{SC} in excess of 34 mA cm^{-2}, *Adv. Mater.*, 2018, **30**, 1704928.

87 H. Aqoma, M. Al Mubarok, W. T. Hadmojo, E. H. Lee, T. W. Kim, T. K. Ahn, S. H. Oh and S. Y. Jang, High-efficiency photovoltaic devices using trap-controlled quantum-dot ink prepared *via* phase-transfer exchange, *Adv. Mater.*, 2017, **29**, 1605756.

88 M. Liu, O. Voznyy, R. Sabatini, F. P. Garcia de Arquer, R. Munir, A. H. Balawi, X. Lan, F. Fan, G. Walters, A. R. Kirmani, S. Hoogland, F. Laquai, A. Amassian and E. H. Sargent, Hybrid organic-inorganic inks flatten the energy landscape in colloidal quantum dot solids, *Nat. Mater.*, 2017, **16**, 258–263.

89 A. H. Ip, A. Kiani, I. J. Kramer, O. Voznyy, H. F. Movahed, L. Levina, M. M. Adachi, S. Hoogland and E. H. Sargent, Infrared colloidal quantum dot photovoltaics *via* coupling enhancement and agglomeration suppression, *ACS Nano*, 2015, **9**, 8833–8842.

90 A. Kiani, B. R. Sutherland, Y. Kim, O. Ouellette, L. Levina, G. Walters, C.-T. Dinh, M. Liu, O. Voznyy, X. Lan, A. J. Labelle, A. H. Ip, A. Proppe, G. H. Ahmed, O. F. Mohammed, S. Hoogland and E. H. Sargent, Single-step colloidal quantum dot films for infrared solar harvesting, *Appl. Phys. Lett.*, 2016, **109**, 183105.

91 J. Z. Fan, M. Liu, O. Voznyy, B. Sun, L. Levina, R. Quintero-Bermudez, M. Liu, O. Ouellette, F. P. García de Arquer, S. Hoogland and E. H. Sargent, Halide re-shelled quantum dot inks for infrared photovoltaics, *ACS Appl. Mater. Interfaces*, 2017, **9**, 37536–37541.

92 J. W. Jo, J. Choi, F. P. García de Arquer, A. Seifitokaldani, B. Sun, Y. Kim, H. Ahn, J. Fan, R. Quintero-Bermudez, J. Kim, M.-J. Choi, S.-W. Baek, A. H. Proppe, G. Walters, D.-H. Nam, S. Kelley, S. Hoogland, O. Voznyy and E. H. Sargent, Acid-assisted ligand exchange enhances coupling in colloidal quantum dot solids, *Nano Lett.*, 2018, **18**, 4417–4423.

93 J. Kim, O. Ouellette, O. Voznyy, M. Wei, J. Choi, M.-J. Choi, J. W. Jo, S.-W. Baek, J. Fan, M. I. Saidaminov, B. Sun, P. Li, D.-H. Nam, S. Hoogland, Z.-H. Lu, F. P. García de Arquer and E. H. Sargent, Butylamine-catalyzed synthesis of nanocrystal inks enables efficient infrared CQD solar cells, *Adv. Mater.*, 2018, **30**, 1803830.

94 J. Choi, J. W. Jo, F. P. G. de Arquer, Y.-B. Zhao, B. Sun, J. Kim, M.-J. Choi, S.-W. Baek, A. H. Proppe, A. Seifitokaldani, D.-H. Nam, P. Li, O. Ouellette, Y. Kim, O. Voznyy, S. Hoogland, S. O. Kelley, Z.-H. Lu and E. H. Sargent, Activated electron-transport layers for infrared quantum dot optoelectronics, *Adv. Mater.*, 2018, **30**, 1801720.

95 M. Liu, F. Che, B. Sun, O. Voznyy, A. Proppe, R. Munir, M. Wei, R. Quintero-Bermudez, L. Hu, S. Hoogland,

A. Mandelis, A. Amassian, S. O. Kelley, F. P. García de Arquer and E. H. Sargent, Controlled steric hindrance enables efficient ligand exchange for stable, infrared-bandgap quantum dot inks, *ACS Energy Lett.*, 2019, **4**, 1225–1230.

96 J. Z. Fan, N. T. Andersen, M. Biondi, P. Todorović, B. Sun, O. Ouellette, J. Abed, L. K. Sagar, M.-J. Choi, S. Hoogland, F. P. G. de Arquer and E. H. Sargent, Mixed lead halide passivation of quantum dots, *Adv. Mater.*, 2019, **31**, 1904304.

97 M.-J. Choi, S.-W. Baek, S. Lee, M. Biondi, C. Zheng, P. Todorovic, P. Li, S. Hoogland, Z.-H. Lu, F. P. G. de Arquer and E. H. Sargent, Colloidal quantum dot bulk heterojunction solids with near-unity charge extraction efficiency, *Adv. Sci.*, 2020, **7**, 2000894.

98 J. Z. Fan, M. Vafaie, K. Bertens, M. Sytnyk, J. M. Pina, L. K. Sagar, O. Ouellette, A. H. Proppe, A. S. Rasouli, Y. Gao, S.-W. Baek, B. Chen, F. Laquai, S. Hoogland, F. Pelayo García De Arquer, W. Heiss and E. H. Sargent, Micron thick colloidal quantum dot solids, *Nano Lett.*, 2020, **20**, 5284–5291.

99 S. Liu, K. Xiong, K. Wang, G. Liang, M.-Y. Li, H. Tang, X. Yang, Z. Huang, L. Lian, M. Tan, K. Wang, L. Gao, H. Song, D. Zhang, J. Gao, X. Lan, J. Tang and J. Zhang, Efficiently passivated PbSe quantum dot solids for infrared photovoltaics, *ACS Nano*, 2021, **15**, 3376–3386.

100 C. Ge, E. Yang, X. Zhao, C. Yuan, S. Li, C. Dong, Y. Ruan, L. Fu, Y. He, X. Zeng, H. Song, B. Hu, C. Chen and J. Tang, Efficient near-infrared PbS quantum dot solar cells employing hydrogenated In_2O_3 transparent electrode, *Small*, 2022, **18**, 2203677.

101 S. Liu, M.-Y. Li, K. Xiong, J. Gao, X. Lan, D. Zhang, L. Gao, J. Zhang and J. Tang, Efficient quantum dot infrared solar cells with enhanced low-energy photon conversion *via* optical engineering, *Nano Res.*, 2023, **16**, 2392–2398.

102 X. Zhao, M. Li, T. Ma, J. Yan, G. M. G. Khalaf, C. Chen, H.-Y. Hsu, H. Song and J. Tang, Stable PbS colloidal quantum dot inks enable blade-coating infrared solar cells, *Front. Optoelectron.*, 2023, **16**, 27.

103 M. Righetto, Y. Wang, K. A. Elmestekawy, C. Q. Xia, M. B. Johnston, G. Konstantatos and L. M. Herz, Cation-disorder engineering promotes efficient charge-carrier transport in $AgBiS_2$ nanocrystal films, *Adv. Mater.*, 2023, e2305009, DOI: **10.1002/adma.202305009**.

104 C. Kim, I. Kozakci, J. Kim, S. Y. Lee and J.-Y. Lee, Highly efficient (>9%) lead-free $AgBiS_2$ colloidal nanocrystal/organic hybrid solar cells, *Adv. Energy Mater.*, 2022, **12**, 2200262.

105 M. G. Ju, J. Dai, L. Ma, Y. Zhou and X. C. Zeng, $AgBiS_2$ as a low-cost and eco-friendly all-inorganic photovoltaic material: nanoscale morphology-property relationship, *Nanoscale Adv.*, 2020, **2**, 770–776.

106 M. Bernechea, N. Cates, G. Xercavins, D. So, A. Stavrinadis and G. Konstantatos, Solution-processed solar cells based on environmentally friendly $AgBiS_2$ nanocrystals, *Nat. Photonics*, 2016, **10**, 521–525.

107 Y. Wang, S. R. Kavanagh, I. Burgués-Ceballos, A. Walsh, D. O. Scanlon and G. Konstantatos, Cation disorder engineering yields $AgBiS_2$ nanocrystals with enhanced optical absorption for efficient ultrathin solar cells, *Nat. Photonics*, 2022, **16**, 235–241.

108 J. Liu, J. Wang, W. Zhao, Z. Zhou and L. Ye, Rise of ecofriendly $AgBiS_2$ nanocrystal solar cells, *Sci. Bull.*, 2023, **68**, 251–254.